Received: 6 June 2016 | Revised: 22 July 2016 | Accepted: 23 July 2016

DOI 10.1002/jemt.22741

RESEARCH ARTICLE

WILEY

Key factors of scanning a plant virus with AFM in air and aqueous solution

Aitziber Eleta-Lopez[1] | **Annalisa Calò**[2]

[1]Self-Assembly Group, CIC nanoGUNE, Tolosa Hiribidea 76, Donostia-San Sebastian, Basque Country 20018, Spain

[2]Nanoscience Iniciative, CUNY Advanced Science Research Center ASRC, 85 St. Nicholas Terrace, New York, New York 10031

Correspondence
Email: a.eleta@nanogune.eu

Review Editor: Prof. Jose Luis Toca-Herrera

Abstract

For tobacco mosaic virus (TMV) as a model virus, this article shows typical issues of scanning soft biological matter by atomic force microscopy (AFM). TMV adsorbed on chemically different flat surfaces, gold, mica, and APDMES-functionalized silicon, is studied in air and aqueous environment. In air, the TMV particles arrangement shows some variety, depending on the substrate. The height of TMV is reduced to 13.7, 15.8, and 15.6 nm, for gold, APDMES, and mica, respectively while the width is about ~30 nm due to the influence of the tip radius. In aqueous solution, the surface charges of the virus and the solid support play an important role in the virus adsorption process. While deposition on negatively charged mica is favored only at low pH values, it is shown that positively charged APDMES functionalized silicon can be a suitable substrate to work with at neutral pHs. The effects of cantilever oscillation's free amplitude (A_0) and the amplitude set-point (A) are also assessed here. While high A_0 prompt reversible deformation of TMV in measurements performed in air, irreversible damage of the virus in liquid conditions (water) is observed using stiff cantilevers (0.35 N m^{-1}) and high A_0 (81 nm), leading to a 6 nm reduction in the height of TMV after the first scan. Finally, low values of the amplitude set-point ($A/A_0 = 0.3$), which means applying higher forces to the sample, also brings the damage of TMV virus assemblies, reducing its monolayer roughness to 0.3 nm.

KEYWORDS

amplitude set-point (A), atomic force microscopy (AFM) in air and aqueous solution, free amplitude (A_0), spring constant (k), Tobacco mosaic virus (TMV)

1 | INTRODUCTION

Viruses have been present on our planet for millions of years but it was not until late XIX century that they were discovered. The first viral entity found was the Tobacco mosaic virus (TMV), a virus that exclusively infects plants (Beijerinck, 1898; Harrison and Wilson, 1999; Iwanowski, 1892; Mayer, 1886). Afterwards, thousands of viruses have been identified which are able to infect plants or animals, fungi, and bacteria.

The majority of viruses consist of an ordered, proteinaceous envelope called capsid that protects the genetic material (DNA or RNA) that is on the interior of the particle. It is said that viruses are "at the edge of life" because they do not replicate by division, like cells. Instead, they replicate using the host cell machinery. Their size varies from <20 nm to hundreds of nanometers and they present different shapes and structures. Virus structure is strictly related to the biological function and it dynamically changes during virus particles formation (self-assembly) or during infections of host cells (Mateu, 2013). Virus structure and physico-chemical properties have been intensely studied to understand infection processes and suppress diseases (Rossmann and Rao, 2012). Also, due to their regular structures, homogeneity and self-assembly ability, they are attractive models for material science and nanotechnology (Calò et al., 2016).

The virus used in this work is the Tobacco mosaic virus (TMV) that infects plants of the family of Solanaceae such us tobacco, tomato or pepper. It causes characteristic mosaic-like patterns, especially on tobacco plants, but it is harmless to mammals. It is a tubular hollow particle where the helical symmetry capsid formed by 2,130 coat proteins surrounds the single-stranded RNA genome. The virus is 300 nm long, has an external surface diameter of 18 nm and a 4 nm wide internal channel (Alonso et al., 2013). Its structure has been very well characterized by means of X-ray diffraction (Kendall et al., 2007) and

cryo-electron microscopy (Clare and Orlova, 2010). TMV is a very versatile and stable virus because of its resilience at extreme conditions at temperature, pH, in solvents, under chemical reactions or pressure (Bonafe et al., 1998; Panyukov et al., 2008; Zaitlin and Israel, 1975). In nanotechnology, TMV has been successfully used to synthetize 1D nanowires, by selectively deposit metal clusters on its external surface or inside the internal channel (Balci et al., 2012; Knez et al., 2004; Wnęk et al., 2013) and 3D nanoarray structures (Gnerlich et al., 2013; Zahr and Blum, 2012). Latest results also show the possibility to use TMV as a drug delivery system for cancer therapy (Czapar et al., 2016).

In the study of virus physico-chemical properties, structure determination techniques played an important role. As mentioned, X-ray diffraction (Bernal and Fankuchen, 1937; Namba and Stubbs 1986) and cryo-electron microscopy (Ge and Hong Zhou, 2011; Sachse et al., 2007) contributed to the study of virus structure at highest resolution (<0.5 nm). Nevertheless, these techniques do not permit to work at physiological conditions. This constitutes a limitation in the study of biological systems in their native environment, a fact that suggests the use of other techniques such as atomic force microscopy (AFM), to investigate the surface of viruses.

The AFM gives the possibility to work on a variety of conditions, from air to vacuum to physiological aqueous environments. With this technique, the nano-structure of the Mason-pfizer monkey virus (Kuznetsov et al., 2007) and Herpex simplex virus capsid (Roos et al., 2009) have been resolved. Also, AFM has been used in the characterization of the mechanical properties of viruses (Zhao et al., 2008), as it is the case of bacteriophage lambda and human adenovirus (Hernando-Pérez et al., 2014; Ortega-Esteban et al., 2015). Thus, atomic force microscopy has become an important technique in virus research.

One of the main issues in analyzing viruses by AFM is related with the sample preparation. It requires the proper immobilization of the particle on a flat surface, which causes the possible alteration of the particle and changes in the aspect ratio due to virus-substrate interactions (Knez et al., 2004). Even more, when working in aqueous solution, the liquid medium can actively influence the immobilization of the particles. Furthermore, in this case weak adsorption may prevent the same sample imaging, as the viruses may move or detach from the surface during scanning (De Pablo and Carrión-Vázquez, 2014). Therefore, the adsorption of the viruses in a controlled way will result from the interplay between the properties of the virus, of the surface and the imaging environment (Armanious et al., 2016).

The AFM amplitude-modulation dynamic mode (also called tapping mode or acoustic mode), differently from the contact mode, is suitable to image soft matter and viruses in air and liquid. Here the tip is not in continuous mechanical contact with the sample, and this reduces lateral forces and the possibility of consequent sample damage compared to contact mode AFM. Here, obtaining a good image requires an accurate control of several parameters beyond the cantilever spring constant and the tip radius, like the resonance frequency and the oscillation amplitude among others (García and Pérez, 2002). Resolution and sample deformation are highly dependent on the cantilever oscillation (oscillation amplitude) selected to operate the instrument.

In amplitude-modulation AFM a piezo actuator makes the cantilever vibrate close to its resonant frequency and at the preselected free amplitude (A_0). When the cantilever approaches the sample, the tip comes into intermittent contact with the surface, and the tip-sample interactions result in the reduction of the oscillation amplitude. A feedback system permits to keep the set-point amplitude constant to obtain the sample topography.

The aim of this work is to discuss the factors that affect the scanning of plant viruses by amplitude-modulation AFM in air and aqueous solution. For that, Tobacco mosaic virus (TMV) has been used as a test sample and deposited on gold, mica and silane-functionalized silicon surfaces. We discuss conditions for adsorption of TMV on these chemically different surfaces in air and in aqueous solutions. Also TMV deformation upon adsorption is described and how this fact influences the particle height and the width (aspect ratio) together with the lateral aggregation and formation of two dimensional virus domains. Finally, we will show drastic conditions resulting in virus damage induced by AFM, in function of relevant parameters in the measurements (cantilever spring constant, free amplitude, amplitude set-point, both in air and aqueous environment).

It has to be noticed that the conditions to scan the same object in amplitude-modulation AFM in air or in aqueous solutions are not the same. The cantilevers used to scan in acoustic mode in air or liquid have different spring constants (k) and resonant frequencies. The range of the most standard cantilever spring constants for air and water measurements vary from $k = 0.02$–40 N m^{-1}. The appropriate choice of the cantilever stiffness/softness is also dependent on the sample nature (Xu et al., 2008). Generally, for measurements in air cantilevers with higher spring constants and resonant frequencies are used compared to measurements in liquid. In our case, because we are working with a soft material, cantilevers with 3 N m^{-1} spring constant and a resonance frequency of about 75 kHz were found as suitable to work in air conditions. In the case of water and water containing ions, due to the viscosity of the liquid, the resonance frequency and the quality factor, (a factor related to the damping of the cantilever in the liquid environment), are reduced compared to air (Moreno-Herrero et al., 2004). In this case we used cantilevers with typical spring constant <0.35 N m^{-1}. The corresponding resonant frequency in air of a cantilever with $k = 0.35$ N m^{-1} is 65 kHz. In aqueous media, we observed a lowering of the resonant frequency and the appearance of several additional peaks in the cantilever frequency spectrum. While values around 10 kHz have been reported for measurements of viruses in water (De Pablo, 2013), for our experiments we observed that working at frequencies between 34 and 36 kHz produced the best results. The appropriate choose of the resonant peak is also a key factor for TMV imaging.

2 | MATERIALS AND METHODS

2.1 | TMV sample preparation

TMV with a concentration of 1 mg L^{-1} in water (strain vulgare) was dialyzed using 10 kDa cut off dialysis filters (slide A lyzer A, 10000

MWCO Thermofisher Scientific). The water was changed six times every 15 min. TMV concentration was adjusted in the range 0.01–0.1 mg mL^{-1}. Depending on the size of the substrate, a droplet between 40 μL (for 0.5 × 0.5 cm^2 substrates) and 100 μL (for 1 × 1 cm^2 substrates) was deposited and left drying on gold and mica surfaces. The samples were placed in a glass petridish overnight at ambient conditions. For experiments carried out in APDMES in liquid, the TMV samples were incubating overnight but in a closed petridish in order to do not dry the droplet. Afterwards, the samples were rinsed with 1 mL of milli-Q water (18 MOhm cm, < 5ppb total organic content, Millipore).

Citrate buffer was used to prepare 0.1 mg mL^{-1} TMV at pH 3.5 and 5.5 using 10 mM citric acid and 10 mM sodium citrate stock solutions (both from Sigma) (Gomori, 1955). Then 20 μL of TMV 1 mg mL^{-1} in water was mixed with 180 μL of buffer, centrifuged at 13,000 rpm (5417C rotor, Eppendorf) for 5 min and 150 μL of the supernatant was substituted by fresh buffer. Between the steps the samples were vortexed to homogenize them. The process was repeated twice.

2.2 | Gold substrate preparation

Flat gold surfaces were prepared on commercial silicon substrates (Silicon Valley SV) by template stripping from annealed gold on mica (SPI Suppliers) (Hegner et al., 1993). Silicon 0.5 × 0.5 cm^2 surfaces were glued (OptiCLEAR SF 850 A&B, Polysciences Inc. 1:1, w:w) face down on commercial 150 nm annealed gold on mica. The gold sandwich was cured at 150°C for 90 min. Then, to obtain finally the flat gold samples, the glued gold/silicon sample border was scratched using sharp tweezers and lifted up. The roughness of the substrate determined by AFM was ~0.5 nm in 1 × 1 μm^2 (see Supporting Information Figure S1). Before incubating TMV, the gold substrates were cleaned by immersion first in acetone (Sigma), then in isopropanol (Sigma) and finally in absolute ethanol (Sigma), for 5 min each. Samples were dried with a nitrogen stream and made hydrophilic by oxygen plasma for 8 min at 1 mbar (standard plasma system femto, Diener Electronics GmbH).

2.3 | APDMES functionalized silicon

Silicon substrates 1 × 1 cm^2 (Silicon Valley SV) were cleaned using the same cleaning procedure as for gold. The silanization was carried out in a glove box in nitrogen atmosphere (Unilab, M-Braun). A 50 μL of 3-(ethoxydimethylsilyl) propylamine 97% (APDMES) (Sigma) was diluted with 4,950 μL toluene (anhydrous, 99.8%) (Sigma). Silicon substrates were dipped in 2 mL APDMES solution and placed in oven at 60°C for 30 min. After functionalization, the surfaces were rinsed twice with toluene and then dried with nitrogen. The roughness measured by AFM was ~0.2 nm in air and in water (see Supporting Information Figure S1). The contact angle was measured using 5 μL milli-Q water by a G10 goniometer (Krüss) in three samples at three different positions. The measured value was ~60° (Terracciano, 2013).

2.4 | Mica

It was cleaved with adhesive tape before depositing TMV. The roughness of mica in air and citrate buffer 10 mM was <0.1 nm (see Supporting Information Figure S1).

2.5 | AFM imaging

AFM images were collected using 5500 AFM (Keysight, Santa Clara). The images in air were taken at ambient conditions with multi75Al tips (Budget Sensor) with 3 N m^{-1} spring constant, a radius <10 nm and nominal fundamental resonant frequency of 75 kHz.

Images in liquid were obtained using citrate buffer 10 mM for experiments at pH 3.5 and pH 5.5 and milli-Q water. DNPS silicon nitride cantilevers (Bruker) were used with $k = 0.35$ N m^{-1} and 0.06 N m^{-1}. The frequency chosen for liquid measurements was in the range 34–36 kHz, considering the peak with the maximum amplitude within the frequency spectrum, and the free amplitude was selected in the range of 40–50 nm. According to the specifications, the nominal value of the tip radius was 20 nm.

All the measurements were carried out in acoustic mode (tapping mode). The free amplitude values were set in volts, and then these values were transformed to nm for each cantilever. For that, amplitude versus distance curves were carried out at $A_0 = 4$V for multi75Al cantilevers in air and at $A_0 = 2$ V for DNPS 0.35 N m^{-1} and DNPS 0.06 N m^{-1} cantilevers in water. In these conditions, we found that for multi75Al A_0 decreases linearly in a range between 2.7 and 0.5 V and for DNPS it decreases linearly between 1.3 and 0.8 V, without discontinuities in the range of $1/4A_0 < A < 3/4A_0$ (García and San Paulo, 2000). We confirmed in this range there was not a change of regime. We fitted the curves with a line obtaining a different slope for different cantilevers. This slope gives reproducible values of the volt (V)/distance (nm) relation for the acoustic mode. We obtained 0.094 V nm^{-1} (multi75Al), 0.057 V nm^{-1} (DNPS, $k = 0.35$ N m^{-1}) and 0.042 V nm^{-1} (DNPS, $k = 0.06$ N m^{-1}). The optical sensitivity in dynamic AFM has been previously calculated from outputs in force reconstruction routines from dynamic experiments (Gadelrab et al., 2013).

All images were taken at 0.7–1 lines per second speed and 512 × 512 pixels. Topography images were treated and the roughness and the profiles analyzed using Gwyddion 2.36 software (www.gwyddion.net). All the images were treated following the same protocol. First the data were leveled by mean plane subtraction, then with a mask all TMV particles were selected and finally the lines in y-axis were corrected by matching height median but excluding the mask region. The z scale was readjusted shifting the minimum data value to zero.

3 | RESULTS

3.1 | TMV imaging in air

Figure 1c and d show typical AFM topographic images of Tobacco mosaic virus (TMV) in air adsorbed on gold and silicon respectively, the latter functionalized with APDMES. The AFM images carried out in acoustic mode show viruses from a suspension of 0.1 mg mL^{-1}

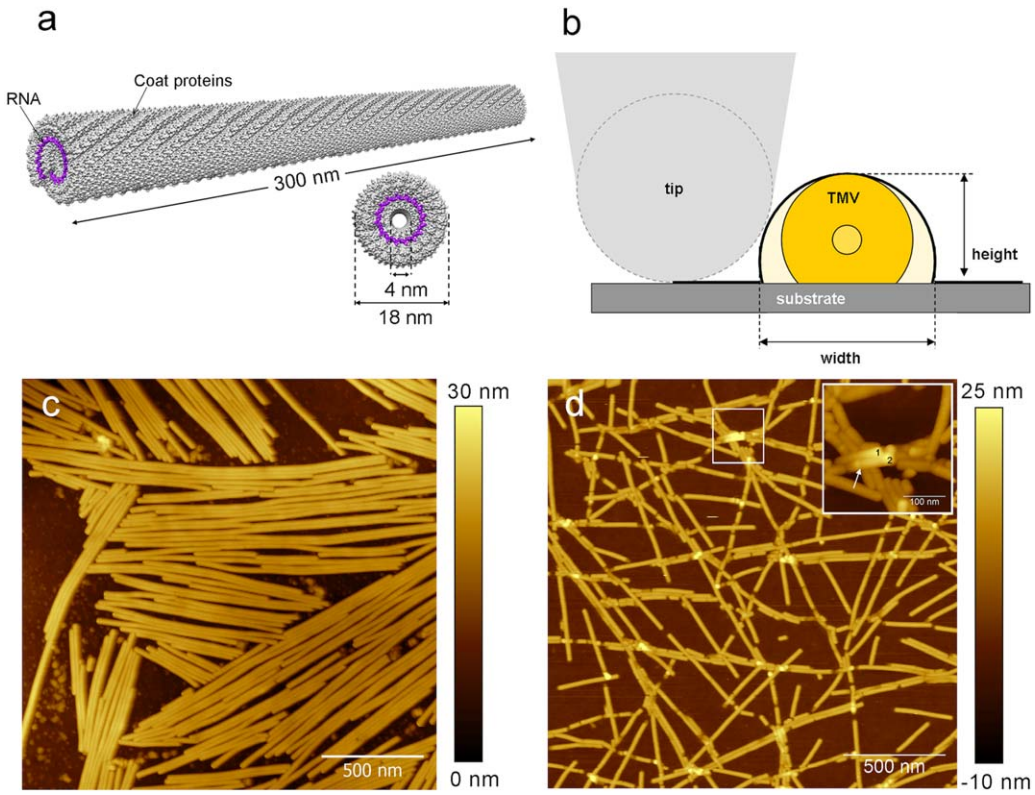

FIGURE 1 (a) Overview of the solid three-dimensional TMV model (300 nm × 18 nm) and the lateral view where 4 nm channel is observed. (b) Illustration of the lateral view of TMV adsorbed on a substrate meanwhile a tip is scanning the surface. The black line drawn at the contour of TMV indicates the width measured from AFM images are larger than expected. (c) TMV 0.1 mg mL^{-1} adsorbed on gold and (d) TMV 0.1 mg mL^{-1} adsorbed on APDMES functionalized silicon. The inset is the high resolution image obtained from the area marked (white square), which is 300 × 300 nm^2 and recorded at 1 line s^{-1} and 512 pixels. There are two viruses labeled as 1 and 2 and the white arrow shows a defect in virus number 2 [Color figure can be viewed in the online issue, which is available at wileyonlinelibrary.com.]

spreading all over the surfaces. In Figure 1a the representation of single TMV particle is shown with its dimensions, which help in its identification in AFM images. As Figure 1c shows, in these conditions TMV particles tend to pack densely on gold. The 300 nm viruses are aligned axially up to 2 μm long rods and at the same time few (three or four) rods assemble in small bundles parallel to their axis, thus forming two dimensional virus domains. Nevertheless, as the topographic image shows, they are not perfectly assembled and so they do not form a complete homogeneous 2D monolayer, as the gaps between the viruses demonstrate.

Figure 1d shows the adsorption of TMV on APDMES functionalized silicon. In this case the TMVs are organized linearly forming long rods structures. Long rods mainly made up of single TMV particles are observed together with isolated single viruses 298 ± 7 nm long. Here viruses tend to organize forming a network of end-to-end interconnected particles. Higher magnification image (see the inset of Figure 1d) shows that the virus network contains also short fragments in the range 25–100 nm.

The thickness of TMV molecules adsorbed on gold and APDMES have been calculated measuring the profiles of the virus from Figure 1c and d. Figure 1b illustrates the lateral view of TMV explaining what we refer as height and width. From our results, the thickness on gold is 13.7 ± 0.1 nm while on APDMES it is slightly larger, 15.6 ± 0.1 nm. These values are lower than the expected value of TMV diameter from X-ray, which is 18 nm.

The inset of Figure 1d shows a high resolution image where a crossing point of several viruses is observed. The viruses marked as 1 and 2 are about 100 nm long, shorter than the expected value of 300 nm, and they are crossing the viruses lying underneath. The profile analysis (see Supporting Information Figure S2) shows that virus number 1 preserves its linear shape, and it is completely straight. Virus designated as number 2 contains a defect (indicated with a white arrow in the inset of Figure 1d) and seems partially bent. This could indicate possible virus damage or irreversible deformation (bending). The highest point of both viruses is closed to 27 nm.

We also measured the full width at half maximum from AFM profiles. For single TMV the width is about 29.7 ± 1.7 nm in gold and 25.3 ± 0.9 nm in APDMES. In both cases viruses are wider than expected because of the influence of the radius of the tip that tends normally to overestimate the lateral size of features in AFM (see Figure 1b). In the case of gold, when we measure the width of several viruses that are organized in parallel (measuring the distance from one virus to the other) we observed that the distance between TMV viruses varies between 16 and 21 nm, with an average width of 18.3 ± 1.9 nm.

When one proceeds to do an AFM measurement in dynamic mode, the frequency and the amplitude of the cantilever should be set. In air, for cantilevers with spring constant of 3 N m^{-1} and a resonance frequency of 75 kHz a value of free amplitude (A_0) of

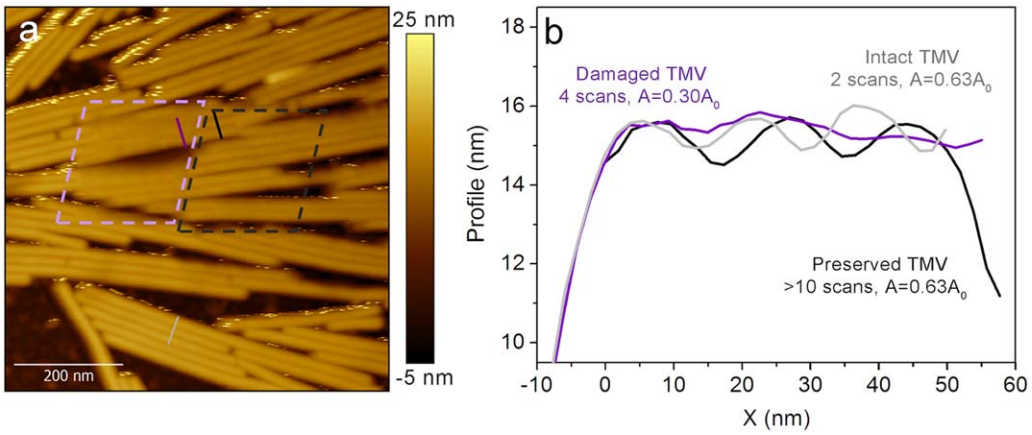

FIGURE 2 (a) AFM topographic image of TMV 0.1 mg mL^{-1} adsorbed on gold. The dashed black square indicates an area scanned with an amplitude set-point (A) 63% of the free amplitude (A_0) and the dashed purple square has been scanned with an amplitude set-point 30% of the free amplitude. The three lines correspond to the profiles that are shown in (b). The purple profile is the area where TMV has been damaged while the black profile indicates the area of TMV that still preserves its shape. Grey profile shows an area that has been scanned only twice at $A = 63\%\ A_0$ [Color figure can be viewed in the online issue, which is available at wileyonlinelibrary.com.]

43 nm was chosen for imaging. Once the cantilever is engaged on the surface at a preset amplitude set-point $A < A_0$, this amplitude set-point defines the force at which the image is performed. Increasing it, the tip is separated from the surface, while very small values for A at the approach could increase the risk of damaging the sample.

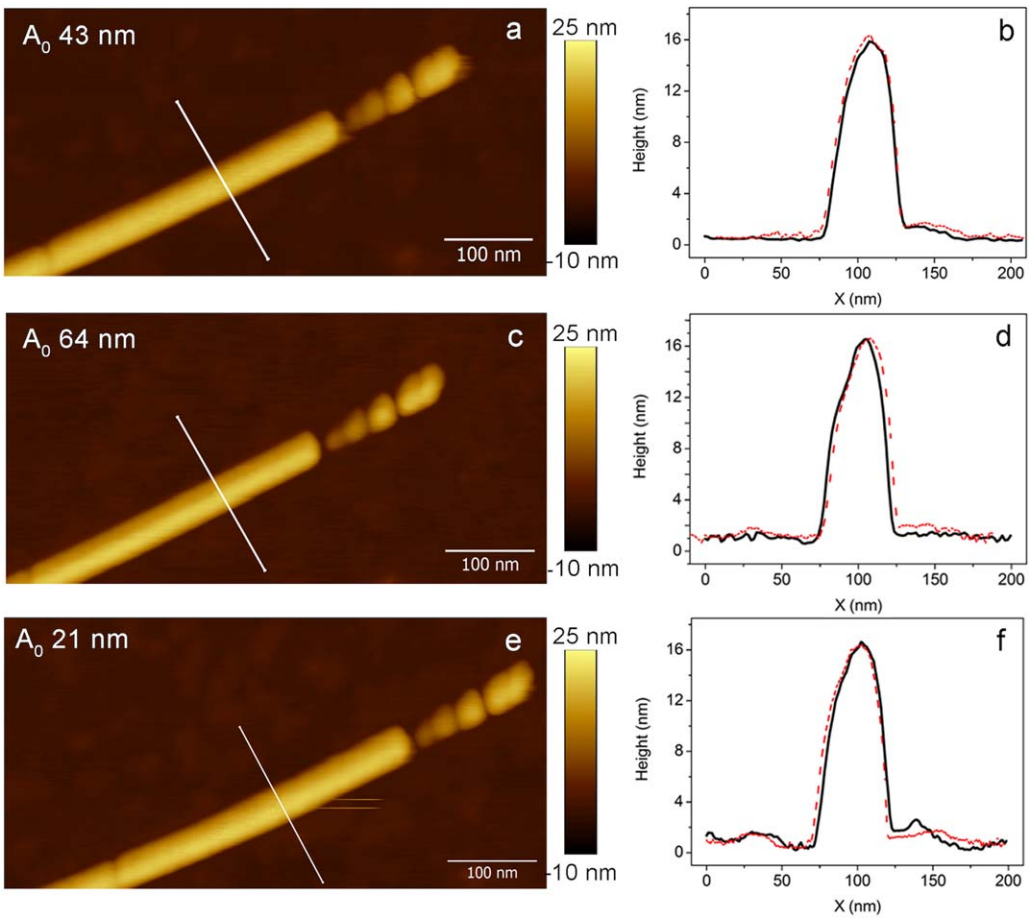

FIGURE 3 (a), (c), and (e) are the topographic AFM images of the same TMV adsorbed on mica. (a) is scanned with a free amplitude (A_0) 43 nm, (b) with $A_0 = 64$ nm and (c) with $A_0 = 21$ nm. (b), (d), and (f) are the profiles corresponding to the white lines in the images, for the first scan (black profiles) and second scan (red dashed profiles). The top right broken pieces here are used as markers [Color figure can be viewed in the online issue, which is available at wileyonlinelibrary.com.]

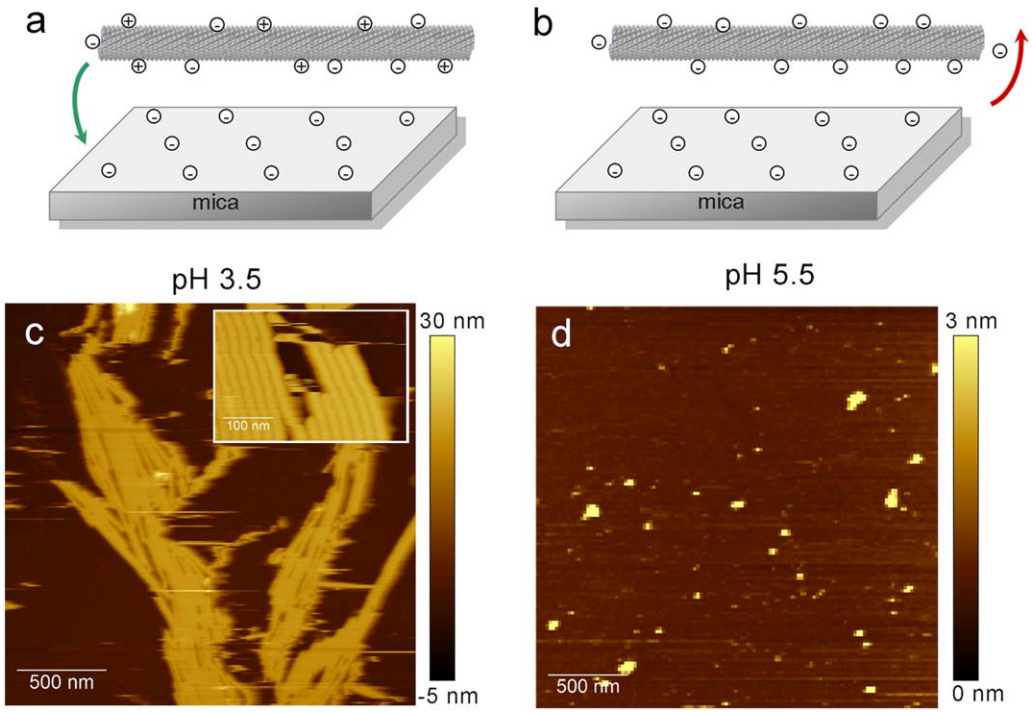

FIGURE 4 Schematic representation of TMV (0.1 mg mL^{-1}) on mica in citrate buffer and corresponding AFM topographic images in citrate buffer 10 mM at pH 3.5 (a), (c) and at pH 5.5 (b), (d). The inset of Figure 4c shows the TMV layer details on mica studied at pH 3.5 but obtained in a different area of the ample area [Color figure can be viewed in the online issue, which is available at wileyonlinelibrary.com.]

The effect of amplitude set-point variation was studied in air and it is shown in Figure 2. TMV 0.1 mg mL^{-1} was deposited on gold in order to have extended TMV monolayers. First the contact between the tip and the surface was established at a preset set-point ($A = 63\%\ A_0$). Then a small area of 300 × 300 nm^2 was scanned (area enclosed in the black square in Figure 2a) with a set-point value $A = 63\%\ A_0$ (27 nm). More than 10 images were carried out sequentially in this area. Then, the area corresponding to the square in purple was scanned with an amplitude set-point decreased to $A = 30\%\ A_0$ (13 nm) and the area was imaged four times. Figure 2 is a larger view of the surface, after these scans [set-point of the image is $A = 63\%\ A_0$ (27 nm)] and shows that the area highlighted in purple scanned at lower set-point value contains damaged viruses, while in the black area the TMV particles are still intact. This is inferred from the topographic profiles in Figure 2b. The black profile differentiates perfectly three viruses while the purple profile shows a deformation of the monolayer surface. Here, the profile on top of the three virus particles appears considerably smoother. The grey profile is related with an area that has been scanned only twice at $A = 63\%\ A_0$ and it shows no differences in comparison with the black profile. Coherently, the root mean square roughness (rms) values calculated for the damaged and not damaged areas show a slight difference, where the rms value of the damaged area is slightly lower than the one where there has not been any deformation. The roughness (rms) values calculated in areas $< 50 \times 50\ nm^2$, are 0.30 ± 0.03 nm for $A = 30\%\ A_0$ and 0.54 ± 0.09 nm for $A = 63\%\ A_0$.

Another critical parameter affecting TMV imaging is the free amplitude of scanning A_0 and is shown in Figure 3. In this case a single virus is studied which was adsorbed on mica. Figure 3a, c, and e show a series of AFM topographic images of the same virus scanned using three different free amplitudes of 43, 64, and 21 nm, respectively. Images were taken sequentially in time, that is, first a, then c and finally e, at the amplitude set-point of $A = 70\%\ A_0$. The virus has been imaged twice to see the effect of the free amplitude on topographic profiles and to assess possible virus damage. Figure 3b, d, f show topographic profiles of TMV. The black line refers to the first image (Figure 3a, c, and e) while the dashed red line refers to the second scanned image. The profiles of the first and second scan images in all the cases demonstrate the virus preserves its shape. However, minor differences are observed depending on the cantilever free oscillation amplitude. The height measured at $A_0 = 43$ nm is 15.6 ± 0.2 nm and the topographic profile in Figure 3b is symmetric. Comparing it with Figure 3d, which corresponds to the scan carried out at $A_0 = 64$ nm, it can be noticed that the left side of the profile has a small hump that is independent on the scan direction. After going back to $A_0 = 21$ nm the virus recovers almost completely its shape. The height at $A_0 = 64$ nm is 15.2 ± 0.4 nm, slightly lower than at $A_0 = 43$ nm, and at $A_0 = 21$ nm it increases to 15.4 ± 0.4 nm and it does not reach exactly the initial values calculated at $A_0 = 43$ nm. This height variability is in the range of the error between topographic heights as determined from images obtained with the same A_0 value. The width has been preserved for all the amplitudes and is 36.2 ± 0.8nm.

3.2 | TMV imaging in aqueous solution

Whenever we study viruses by AFM in aqueous solution the role of the liquid itself is an important factor that will determine first the adsorption

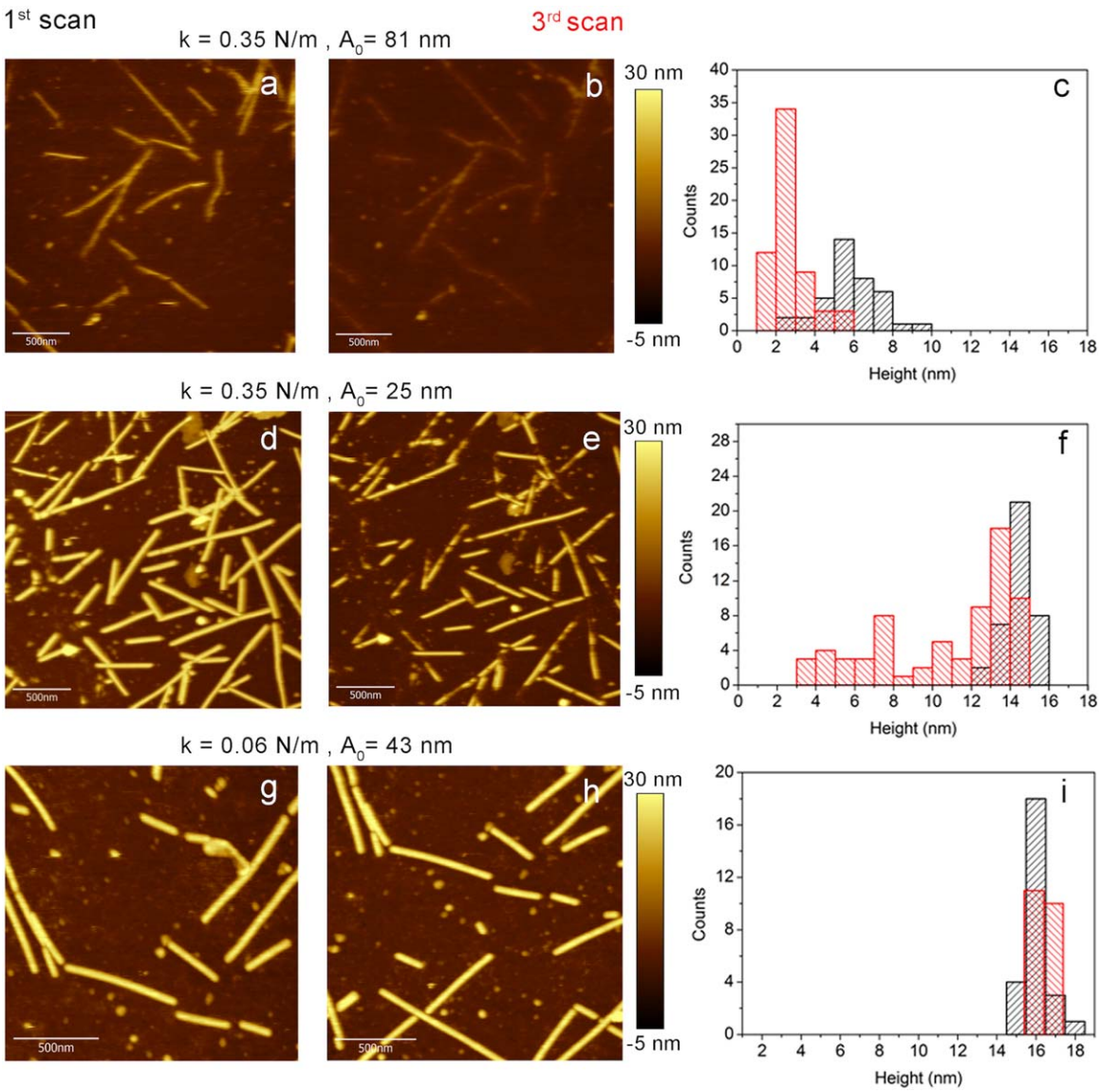

FIGURE 5 AFM topographic images of TMV 0.01 mg mL^{-1} adsorbed on APDMES and scanned in water. (a), (b): cantilever has spring constant 0.35 N m^{-1} and imaging is performed at $A_0 = 81$ nm. (d), (e): spring constant is 0.35 N m^{-1} and $A_0 = 25$ nm .(g, h): spring constant is 0.06 N m^{-1} and $A_0 = 43$ nm. (a), (d), and (g) are images of the first scan and (b), (e), and (h) the images of the same area after the third scan. (c), (f), and (i) are the height distribution histograms obtained measuring the topographic height of 50–65 particles. The black values refer to the first scan while the red values to the third scan [Color figure can be viewed in the online issue, which is available at wileyonlinelibrary.com.]

of the particle and stability on the surface and also affects the scanning of the sample due to interactions between tip and sample.

Figure 4 shows AFM images obtained after depositing TMV (0.1 mg mL^{-1}) on mica in citrate buffer 10 mM. The pH of the buffer has been varied from pH 5.5 (Figure 4d) to pH 3.5 (Figure 4c). At pH 5.5 there are not particles deposited on the surface, as it is shown in Figure 4d. In this condition, both TMV and mica are negatively charged and, due to repulsive interactions, TMV cannot be deposited on the surface. As the pH of the buffer is decreased to 3.5, the TMV isoelectrical point is reached (Alonso et al., 2013) and the charge distribution at the TMV surface changes. In this condition, the number of positive charges equals that of negative charges at the TMV surface. Thus, TMV can be deposited on mica and assembles end-to-end and side-by-side forming two dimensional ordered domains (see Figure 4c), similar to those observed on gold in dry conditions. Single TMV particles were not observed. A detail is shown in the inset of Figure 4c. Figure 4a and b are schematics indicating the surface charge on both TMV and mica that determines the adsorption. Even if we did not perform a systematical analysis varying the pH, our results demonstrate that this parameter is crucial for imaging TMV by AFM in aqueous conditions, and that mica is not a good surface for TMV adsorption to work with at pH $\geq$ 5.5.

An alternative substrate that is positively charged at neutral pH has been selected to adsorb TMV. This surface was obtained by functionalizing a silicon substrate with APDMES (3-(ethoxydimethylsilyl) propylamine), containing amine groups which are positively charged working in water (see Figure 5). In Figure 5g low TMV concentration of

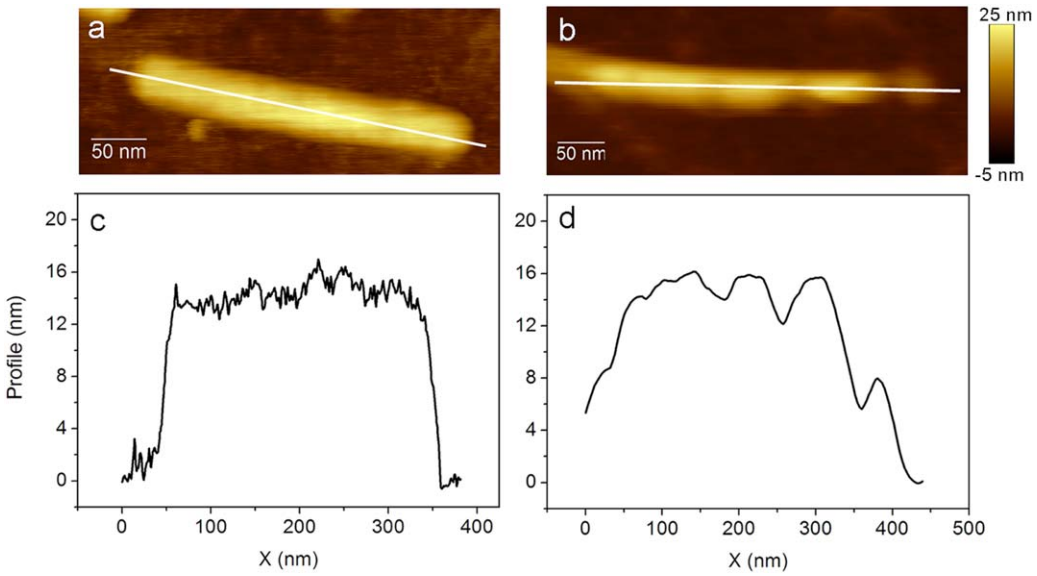

FIGURE 6 (a) Not damaged TMV virus adsorbed on APDMES and scanned with a cantilever with $k = 0.06$ N m^{-1} and (c) its profile indicated by a white line in (a). (b) Damaged TMV particle also adsorbed on APDMES and scanned with a cantilever with $k = 0.35$ N m^{-1} and (d) profile corresponding to the white line in (b). [Color figure can be viewed in the online issue, which is available at wileyonlinelibrary.com.]

0.01 mg mL^{-1} has been used, so individual particles are visible and few of them are assembled end-to-end forming long rods. The height calculated from the profiles of the corresponding images show that the thickness of TMV on mica at pH 3.5 is 17.7 ± 0.1 nm (Figure 4c) and the height of TMV on APDMES is 16.1 ± 0.7 nm. Regarding the width on mica and at pH 3.5, we calculated it from areas where TMV is well aligned and assembled, measuring the distance from particle to particle. In this case it varies from 19 to 22 nm, being the average value 21.6 ± 0.8 nm. The width of individual particles on APDMES is 44.5 ± 3.1 nm, a value higher than the particles scanned in air due to the influence of the tip radius. The nominal value of the tip radius for the cantilevers used in aqueous experiments is 20 nm while in air it is $<$10 nm. Thus, our results show that unlike the mica, positively charged APDMES is better substrate for the adsorption of TMV at neutral pHs.

Choosing a proper tip is an important factor to work in liquids with soft matter. In general, the tips used in aqueous solution for tapping mode have lower spring constant than the ones in air. In a first attempt we used a tip with a spring constant one order of magnitude lower than the ones used in air ($k = 0.35$ N m^{-1}). The frequency also should be carefully selected, because while in air a well definite peak results from the tune of the fundamental resonance frequency, in liquid conditions several and broader peaks appear. For our cantilevers and instrument choosing a frequency at 34–36 kHz gave good results.

In Figure 5, the effect of the free amplitude in TMV imaging in liquid on APDMES substrate is shown. Figures 5a, b, d, e show the first (a, d) and third (b, e) scans carried out at the same position with tips having $k = 0.35$ N m^{-1} and at a set-point amplitude that is the 72% of the free amplitude. Figures 5a and b have been obtained using a free amplitude $A_0 = 81$ nm. The AFM images and the histogram in Figure 5c clearly show that since the first scan (black columns of the histogram) the tip damages the virus irreversibly, being the TMV maximum height distribution 5.5 nm. At the third scan (red columns of the histogram) the height decreases to 2.5 nm. Reducing the free amplitude from 81 to 25 nm an improvement is observed (see Figure 5d and e). The maximum in the height distribution histogram (Figure 5f black columns) corresponds to 14.5 nm during the first scan. At the third scan this maximum shifts to 13.5 nm. Also the contribution to the total histogram of heights comprised between 3 and 12 nm indicates that some particles appear highly deformed under tip scanning. This damage is irreversible. In fact, lowering the free amplitude to $A_0 = 10$ nm after the second scan we still observed a lower topographic height with an average maximum value around 13.9 ± 2.2 nm (see Supporting Information Figure S3). The preservation of the TMV height was observed in milder conditions, that is, using ten times softer cantilevers with a spring constant 0.06 N m^{-1} and using $A_0 = 42$ nm for imaging. This is observed in Figure 5g and h. The viruses preserved their shape and the histogram of Figure 5i demonstrates that the virus height is constant at 16.1 ± 0.7 nm even after few scans. Lower A_0 implies lower forces are applied to the sample, together with a lower energy dissipation and tip-sample contact time during each oscillation cycle (Cleveland et al., 1998; García and San Paulo, 2000).

Details of the TMV virus damage on APDMES are captured in Figure 6. A virus that is not damaged (conditions $k = 0.06$ N m^{-1} and $A_0 = 23$ nm) preserves its dimensions after scanning, i. e. the expected 300 nm length and the 16 nm height expected for TMV on APDMES. The profile of Figure 6c refers to the image in Figure 6a and shows a relatively flat surface. However, when a larger force is applied (conditions $k = 0.35$ N m^{-1} and $A_0 = 26$ nm) the virus surface presents irreversible damages, as the image in Figure 6b and profile in Figure 6d demonstrate. The damage results in a heterogeneous profile, that is, bumps along the TMV structure, giving rise to regions of alternating higher and lower heights, in an aberrant aspect ratio (height/width) and

in a curved shape indicating virus deformation. In the profile of Figure 6d the decrease in the height along the profile is clear. Further investigations will be carried out by means of high resolution imaging to study if specific regions in the virus structure are more sensitive to the tip scan.

4 | DISCUSSION

AFM study of TMV in air and liquid presents main issues. AFM characterization requires the virus being strongly attached to the surface, a condition that can be difficult to achieve especially in liquid conditions, due to electrostatic forces between charged species at the surface of the substrate and of the virus particle. The interaction between the substrate and the virus should be stronger than interaction between the tip and the virus, in order to avoid virus detachment and shear during scanning. Furthermore, the force applied during the scan should be adjusted avoiding virus damage, to obtain good quality images.

In this work three different substrates have been used for TMV deposition, that is, gold, mica, and APDMES functionalized silicon. For experiments in air, the adsorption of TMV on hydrophilic gold and mica is carried out by evaporation of a drop containing suspended viruses. This results in the deposition of all the particles on the surface. Here, it is important to choose the proper TMV concentration but also to have a clean suspension, free of salts, in order to not contaminate the samples, thus affecting the quality of the AFM images in air. However, working at environmental conditions one has to take into account there is always an ultrathin water layer of nearly molecular thickness practically on all substrates and surfaces that can influence the adsorption and the correct determination of the sample topography by AFM (Santos et al., 2012; Verdaguer et al., 2012).

In aqueous solution water and ions play an important role and affect the substrate-virus interaction. This is clearly observed in Figure 4, where in citrate buffer at pH 5.5, due to the electrostatic repulsion between negative charges on both mica and TMV surfaces, it is impossible to adsorb TMV on mica. Because TMV is stable in a wide range of pHs (Alonso et al., 2013), we were able to decrease the pH till reaching the TMV isoelectric point at pH 3.5. In this condition, the TMV overall charge is zero, positive, and negative charges compensate, while mica is still negatively charged. In fact, the isoelectric point of mica is at pH 3 (Roiter et al., 2006), meaning that the negative charge density on this surface is higher at pH 5.5 than at pH 3.5. To improve the TMV adsorption for scanning at physiological conditions or neutral conditions, another strategy has to be carried out. In this case functionalizing the surface with an amino-terminal silane, which is positively charged at neutral pH, is a good strategy. As it is demonstrated in Figure 5, the electrostatic interactions between substrate and negatively charged virus favor TMV adsorption on this positively charged surface.

On gold and in air, TMV tend to assemble axially forming two dimensional domains (Figures 1c and 2a). The concentration of TMV will determine the extent of such assemblies in *xy*. In contrast, it is observed that on APDMES TMV is mostly found as single particle, if the concentration is low or it is assembled in long, rod-like structures at higher concentrations (see Figure 1d). One of the reasons is the sample preparation method. In the case of gold, the TMV sample is prepared by complete evaporation of the suspension which means that, apart from the substrate/virus interactions, drying effects (water evaporation) also influence the formation of such assemblies. Meanwhile, in the case of APDMES the system is left in the aqueous suspension in a closed environment to avoid the drop gets dried. In the latest case, the adsorption will be driven only by interactions between the substrate and the TMV, which is mainly electrostatic in nature (amine groups of APDMES and negatively charged TMV in water). Both substrate and deposition protocol affect the final aggregation of TMV, where APDMES favors end-to-end linear aggregation of the virus and gold the side-by-side aggregation, giving rise to bundles. On the other hand, in liquid the difference between mica and APDMES (where in mica are observed bundles and in APDMES single TMV particles) could also depend on the surface charge. When the charge on the surface is negative (mica) interactions between neutral single viruses are facilitated and one can see 2D aggregation in layers. On APDMES the virus is attracted by the opposite charge of the surface, but single viruses (negatively charged) do not tend to interact between each other. So the layered structure is not observed.

On the other side, the original dimensions of the virus, 300 nm in length and 18 nm in diameter, are modified once viruses are adsorbed. In particular, on APDMES surfaces (see Figure 1d) single viruses were observed with varying length from 300 to 100 nm, or even smaller. This means that these viruses have been partially split upon adsorption. This fact has been already observed on hydrophobic surfaces (Britt et al., 1998) and later on graphene (Dubrovin et al., 2004). Britt et al. carried out a kinetic study of TMV adsorption on organic monolayers, observing that, while both electrostatic and hydrophobic interactions influence TMV adsorption, only in the case of hydrophobic surfaces viral disassembly and shortening occurs. In our case, this effect was observed on a positively charged surface. Further experiments are necessary to clarify the mechanism behind the shortening of TMV particles on APDMES or on positively charged surfaces. Anyway it is interesting to notice that the generally recognized mechanism of TMV disassembly is electrostatic in nature and it is mediated by positive ions. When a virus enters in a plant cell, protons and calcium ions are removed from the virus capsid and this destabilizes the structure of the coat proteins. The disassembly is initiated at specific carboxylates residues inside the coat proteins (Glu50, Asp77, Glu95, and Glu106) that are coordinated by calcium ions (Stubbs, 1999). It is possible that the positively charged APDMES structure interferes with the tertiary structure of the coat proteins in TMV (Alonso et al., 2013).

The height of adsorbed TMV varies with the substrate, as reported in previous works. In all the experiments shown in this work, the measured TMV height is lower than the TMV diameter (18 nm). The lowest values were obtained in air for hydrophilic mica and gold with values of 15.6 and 13.7 nm, respectively. For APDMES (water droplet CA 60°), which is more hydrophobic substrate compared to mica and gold (water droplet CA $< 5°$ for mica and gold), the measured height in air is 15.8 nm which is similar to the values obtained for hydrophilic mica. It

is known that the reason of a reduced height of the virus at hydrophilic substrates is due to the formation of hydrogen bonds. Furthermore, in previous works it has been reported that for hydrophobic graphite (HOPG, water droplet CA 90°) the deformation is minimal and values close to 18 nm due to Van der Waals interactions between the graphite and the virus were obtained (Dubrovin et al., 2004; Knez et al., 2004; Lee et al., 2008). For APDMES in water we obtained 16.1 nm and in the case of TMV on mica scanned at pH 3.5 (citrate buffer 10 mM) the height calculated was closer to the TMV diameter, 18 nm. This height difference also could be associated with the surface charge. In other words, negatively charged TMV is attracted more strongly to positively charged APDMES (in water) than neutral TMV to negatively charged mica (at pH 3.5). These observations point out that electrostatic interactions may play an important effect on the virus geometry upon adsorption.

In contrast to the vertical resolution, the AFM tends to overestimate the lateral dimensions due to the tip radius. This occurs when the object under test and the tip have similar dimensions, therefore one obtains always wider values than expected (De Pablo, 2013; Trinh et al., 2011). In single TMV particles, instead of 18 nm width, about 30 nm is measured in air with tips of radius <10 nm. In liquid, the measured width is 44 nm and tip radius is 20 nm. The larger the tip radius the larger the lateral size of the scanned TMV. In contrast, when viruses are laterally aggregated in bundles in air, the width of single viruses appeared lower. In our measurements the width of the virus assemblies on gold varies between 16 and 21 nm. Similar variation has been observed also on mica (see Supporting Information Figure S4). Maeda (1997) reported a width of 14.7 nm for uniaxially oriented TMV domains. These observations indicate that generally the TMV particles get compressed when they interact along the main tube axis and when they are arranged in bundles. Also at pH 3.5 (see Figure 4) the TMV-TMV distance has been measured to be between 19 and 22 nm, indicating a slight compression compared to isolated viruses. In all the cases, the virus width is larger than 18 nm (see Supporting Information Figure S5). The use of sharper tips may give rise to less wider features. Anyway, previous reports showed virus deformation using sharp cantilevers (Vesenka et al., 1993).

For imaging viruses in air, cantilevers with higher spring constants produced the best images, while for imaging in liquid cantilevers one order of magnitude softer have been used. Even if the TMV is known to have a high mechanical resistance (Falvo et al., 1997) (measurements of the Young's modulus of 1GPa in TMV has been measured by means of cantilevers with $k = 20–70$ N m^{-1}), the best images in air were obtained with relatively soft cantilevers with $k = 3$ N m^{-1} ($f = 75$ kHz). In liquid, cantilevers with spring constant ≤ 0.35 N m^{-1} can be used to image TMV. The best results were obtained with very soft cantilevers with 0.06 N m^{-1} spring constant (see Figure 5).

Sample deformation is highly dependent on the cantilever oscillation. The effect of the imaging amplitude (free amplitude, amplitude set-point) was studied here for both dry and liquid imaging (see Figure 2, 3, and 5). With respect to the free amplitude, the same virus has been scanned twice in air, varying this parameter from 43 to 64 nm and returning to 21 nm. The results show (Figure 3) that the virus can stand all the scans and scanning it at $A_0 = 64$ nm results in a slight reversible deformation of the virus that is completely recovered rescanning its surface again at $A_0 = 21$ nm. In liquid, variations of the free amplitude from $A_0 = 81$ nm to $A_0 = 25$ nm are very critical (see Figure 5). At high amplitude the virus is completely destroyed since the first scan, while the lower is the amplitude the better the virus resists the scans. However, we observed that even at very low free amplitudes, as $A_0 = 10$ nm, still some viruses are damaged by the tip (see Supporting Information Figure S3). This implies best imaging conditions can be obtained applying very small forces or lowering the stiffness of the cantilever. Here we proved that in conditions of $k = 0.06$ N m^{-1} and $A_0 = 40–50$ nm virus integrity is preserved. It has to be noticed that our experiments were carried out with cantilevers with specific chemistry, that is, with silicon (for air measurements) and silicon nitride (for liquid measurements) cantilevers. It is well known that the force between tip-substrate can also depend on the cantilever surface chemistry (Tsukruk and Bliznyuk, 1998). Changing the chemistry by tip functionalization might influence not only the type of forces exerted on the sample, but also the dependence of the measured TMV height and width on the scanning parameters and the entity of the irreversible sample deformation under drastic scanning conditions. These aspects will be elucidated in further studies.

When the tip is engaged to the sample, the set-point amplitude is the value that the feedback loop keeps constant and that is used to record the topography in the acoustic mode. Increasing the imaging set-point the contact with the sample is lost and it is impossible to collect any image. If the set-point is too low the risk to damage the sample increases. This is shown in Figure 2. When the set-point is decreased by 70% of the free amplitude, we started observing damage in the scanned area. The control of this parameter is important for imaging, because it determines the actual force applied on the sample and in the case of soft materials it is crucial for avoiding sample damage. In some cases, viruses disappeared during scanning in liquid; leaving only some traces on the surface (see Figure 5). Nevertheless, the removed material is not accumulated in the scan area, meaning that it goes outside this area or into the solution. Surprisingly, the same tip could be used during the experiment, and this indicates that the virus is not attached on the tip.

5 | CONCLUSIONS

This study gives insights about the factors that influence the scanning of a biological soft sample by AFM in air and aqueous solutions. For that, a model plant virus has been used, Tobacco mosaic virus (TMV), which has been immobilized on flat solid supports. Depending on the substrate chemistry and the experimental conditions, the TMV particles assemble forming different two dimensional arrangements. The presence of the substrate always results in the partial deformation of the virus. In air, it is observed that the height of the virus decreases from the expected value of 18 nm to a value comprised between 13 and 16 nm due to the hydrogen bonding formed on hydrophilic gold or

mica and the electrostatic interactions between APDMES and the virus. In liquid, adsorbing TMV on mica and working at pH 3.5, the virus preserves its height close to 18 nm. In all the cases the width of single viral particles is larger because of the influence of the tip radius.

The selection of a proper cantilever is a key point to avoid sample damage while scanning. In particular, the proper choose of the cantilever spring constant depending on the scanning conditions (imaging in air or in aqueous solutions) is addressed in this work. At high free amplitudes (A_0) viruses were deformed partially and reversibly in air. This parameter becomes very critical in aqueous solution where the viruses are damaged irreversibly. Regarding the amplitude set-point, a compromise must be found when setting this value while operating the microscope, in order to obtain images of good resolution without damaging the sample. In high resolution images of TMV, we observed that virus damage occurs at specific points on its surface. The mechanism behind AFM-induced virus damage and its relation with the TMV structure needs to be elucidated and will be systematically addressed in further investigations.

ACKNOWLEDGMENTS

The authors thank the support of the Basque Government with the project PI2013-57, Gipuzkoako Foru Aldundia under the project Nanoscopía Mojada (PCTi 2015) and the project Fibras Fluidas – RETOS of the Spanish Government (MINECO). TMV solutions were provided by the group of Prof. Christina Wege (Institute for Biomaterials and Biomolecular Systems, University of Stuttgart). The authors also thank Prof. Alexander M. Bittner for discussion and corrections of the manuscript and Dr. Mitsuhiro Okuda for helping with TMV 3D model.

REFERENCES

Alonso, J. M. & Górzny M. Ł., Bittner, A. M. (2013). The physics of tobacco mosaic virus and virus-based devices in biotechnology. *Trends in Biotechnology*, *31*, 530–538.

Armanious, A., Aeppli, M., Jacak, R., Refardt, D., Sigstam, T., Kohn, T., & Sander, M. (2016). Viruses at solid–water interfaces: A systematic assessment of interactions driving adsorption. *Environmental Science and Technology*, *50*, 732–743.

Balci, S., Hahn, K., Kopold, P., Kadri, A., Wege, C., Kern, K., & Bittner, A. M. (2012). Electroless synthesis of 3 nm wide alloy nanowires inside tobacco mosaic virus. *Nanotechnology*, *23*, 045603–045610.

Beijerinck, M. W. (1898). Über ein contagium vivum fluidum als ursache der fleckenkrankheit der Tabaksblätter. *Verh Kon Akad Wetensch*, *5*, 3–21.

Bernal, J. D. & Fankuchen, I. (1937). Structure types of protein "crystals" from virus-infected plants. *Nature*, *139*, 923–924.

Bonafe, C. F., Vital, C. M., Telles, R. C., Gonçalves, M. C., Matsuura, M. S., Pessine, F. B., Freitas, D. R., & Vega, J. (1998). Tobacco mosaic virus disassembly by high hydrostatic pressure in combination with urea and low temperature. *Biochemistry*, *37*, 11097–11105.

Britt, D. W., Buijs, J., & Hlady, V. (1998). Tobacco mosaic virus adsorption on self-assembled and langmuir-blodgett monolayers studied by TIRF and SFM. *Thin Solid Films*, *327–329*, 824–828.

Calò, A., Eiben, S., Okuda, M., & Bittner, AM. (2016). Nanoscale device architectures derived from biological assemblies: The case of tobacco mosaic virus and (apo)ferritin. *Japanese Journal of Applied Physics*, *55*, 03DA01_1:17.

Clare, D. K. & Orlova, E. V. (2010). 4.6 é Cryo-EM reconstruction of tobacco mosaic virus from images recorded at 300 keV on a 4k×4k CCD camera. *Journal of Structural Biology*, *171*, 303–308.

Cleveland, J. P., Anczykowsky, B., Schmid, A. E., & Elings, V. B. (1998). Energy dissipation in tapping-mode atomic force microscopy. *Applied Physics Letters*, *72*, 2613–2615.

Czapar, A. E., Zheng, Y. R., Riddell, I. A., Shukla, S., Awuah, S. G., Lippard, S. J., & Steinmetz, N. F. (2016). Tobacco mosaic virus delivery of phenanthriplatin for cancer therapy. *ACS Nano*, *10*, 4119–4126.

De Pablo, P. J. & Carrión-Vázquez, M. (2014). Imaging biological samples with atomic force microscopy. *Cold Spring Harbour Protocols*. *2*, 168–177.

De Pablo, P. J. (2013). Atomic force microscopy of viruses. In M. G. Mateu (Ed.), *Structure and physics of viruses: An integrated textbook* (pp. 247–271). London: Springer.

Dubrovin, E. V., Kirikova, M. N., Novikov, V. K., Drygin, Y. F., & Yaminsky, I. V. (2004). Study of peculiarities of adhesion of tobacco mosaic virus by atomic force microscopy. *Colloid Journal*, *66*, 750–755.

Falvo, M. R., Washburn, S., Superfine, R., Finch, M., Brooks, F. P., Chi, V. Jr., & Taylor, R. M. II. (1997). Manipulation of individual viruses: Friction and mechanical properties. *Biophysical Journal*, *72*, 1396–1403.

Gadelrab, K. R., Santos, S., & Chiesa, M. (2013). Heterogeneous dissipation and size dependencies of dissipative processes in nanoscale Interactions. *Langmuir*, 20:2200–2206.

García, R. & Pérez, R. (2002). Dynamic atomic force microscopy methods. *Surface Science Reports*, *47*, 197–301.

García, R. & San Paulo, A. (2000). Amplitude curves and operating regimes in dynamic atomic force microscopy. *Ultramicroscopy*, *82*, 79–83.

Ge, P. & Hong Zhou, Z. (2011). Hydrogen bonding networks and RNA bases revelaed by cryo electron microscopy suggest a triggering mechanism for calcium switches. *Proceedings of the National Academy of Science USA*, *108*, 9637–9642.

Gnerlich, M., Pomerantseva, E., Gregorczyk, K., Ketchum, D., Rubloff, G., & Ghodssi, R. (2013). Solid flexible electrochemical supercapacitor using tobacco mosaic virus nanostructures and ALD ruthenium oxide. *Journal of Micromechanics and Microengineering*, *23*, 114014–111421.

Gomori, G. (1955). Preparation of buffers for use in enzyme studies. *Method Enzymology*, *1*, 138–146.

Harrison, B. D. & Wilson, T. M. A. (1999). Milestones in research on tobacco mosaic virus. *Philosophical Transactions of the Royal Society of London: Series B Biological Sciences*, *354*, 521–529.

Hegner, M., Wagner, P., & Semenza, G. (1993). Ultralarge atomically flat template-stripped au surfaces for scanning probe microscopy. *Surface Science*, *291*, 39–46.

Hernando-Pérez, M., Lambert, S., Nakatani-Webster, E., Catalano, C. E., & De Pablo, P. J. (2014). Cementing proteins provide extra mechanical stabilization to viral cages. *Nature Communications*, *5*, 4520–45027.

Iwanowski, D. I. (1892). Über die mosaikkrankheit der Tabakspflanze. *Bulletin de l'Academie Imperiale des Sciences de St Petersburg*, *35*, 65–70.

Kendall, A., McDonald, M., & Stubbs, G. (2007). Precise determination of the helical repeat of tobacco mosaic virus. *Virology*, *369*, 226–227.

Knez, M., Sumser, M., Bittner, A. M., Wege, C., Jeske, H., Martin, T. P., & Kern, K. (2004). Spatially selective nucleation of metal clusters on the tobacco mosaic virus. *Advanced Functional Materials*, *14*, 116–124.

Knez, M., Sumser, M. P., Bittner, A. M., Wege, C., Jeske, H., Hoffmann, D. M. P., Kuhnke, K., & Kern, K. (2004). Binding the tobacco mosaic virus to inorganic surfaces. *Langmuir*, *20*, 441–447.

Kuznetsov, Y. G., Ulbrich, P., Haubova, S., Ruml, T., & McPherson, A. (2007). Atomic force microscopy investigation of mason–pfizer monkey virus and human immunodeficiency virus type 1 reassembled particles. *Virology*, *360*, 434–446.

Lee, B., Lo, C. T., Thiyagarajan, P., Winans, R. E., Li, X., Niu, Z., & Wang, Q. (2008). Effect of the interfacial interaction on the cross sectional morphology of tobacco mosaic virus using GISAXS. *Langmuir*, *23*, 11157–11163.

Maeda, H. (1997). An atomic force microscopy study for the assembly structures of tobacco mosaic virus and their size evaluation. *Langmuir*, *13*, 4150–4161.

Mateu, M. G. 2013. *Structure and physics of viruses: An integrated textbook (p 3)*. London: Springer.

Mayer, A. (1886). Über die mosaikkrankheit des Tabaks. *Landw Vers Sta*, *32*, 451–467.

Moreno-Herrero, F., Colchero, J., Gómez-Herrero, J., & Baró, A. M. (2004). Atomic force microscopy contact, tapping, and jumping modes for imaging biological samples in liquids. *Physical Review E*, *69*, 031915–031923.

Namba, K. & Stubbs, G. (1986). Structure of tobacco mosaic virus at 3.6é resolution: Implications for assembly. *Science*, *231*, 1401–1406.

Ortega-Esteban, A., Condezo, G. N., Pérez-Berná, A. J., Chillón, M., Flint, S. J., Reguera, D., San Martín, C., & de Pablo, P. J. (2015). Mechanics of viral chromatin reveals the pressurization of human adenovirus. *ACS Nano*, *9*, 10826–10833.

Panyukov, Y. V., Nemykh, M. A., Dobrov, E. N., & Drachev, V. A. (2008). Surfactant-induced amorphous aggregation of tobacco mosaic virus coat protein: A physical methods approach. *Macromolecular Biosciences*, *8*, 199–209.

Roiter, Y., Jaeger, W., & Minko, S. (2006). Conformation of single polyelectrolyte chains vs. salt concentration: Effects of sample history and solid substrate. *Polymer*, *47*, 2493–2498.

Roos, W. H., Radtke, K., Kniesmeijer, E., Geertsema, H., Sodeik, B., & Wuite, G. J. (2009). *Proceedings of the National Academy of Sciences USA*, *106*, 9673–9678.

Rossmann, M. G. & Rao, V. B. (2012). *Viral molecular machines*. London: Springer.

Sachse, C., Chen, J. Z., Coureux, P. D., Stroupe, M. E., Fändrich, M., & Grigorieff, N. (2007). High resolution electron microscopy of helical specimens: A fresh look at tobacco mosaic virus. *Journal of Molecular Biology*, *371*, 812–835.

Santos, S., Verdaguer, A., & Chiesa, M. (2012). The effect of adsorbed water layers on the apparent height of nanostructures in ambient amplitude modulation atomic force microscopy. *Journal of Chemical Physics*, *137*, 044201_1:14.

Stubbs, G. (1999). Tobacco mosaic virus particle structure and the initiation of disassembly. *Philosophical Transactions of the Royal Society of London: Series B Biological Sciences*, *354*, 551–557.

Terracciano, M. (2013). Optical characterization of aminosilane-modified silicon dioxide surface for biosensing. *Journal of the European Optical Society—Rapid Publications*, *8*, 13075–13080.

Trinh, M. H., Odorico, M., Bellanger, L., Jacquemond, M., Parot, P., & Pellequer, J. L. (2011). Tobacco mosaic virus as an AFM tip calibrator. *Journal of Molecular Recognition*, *24*, 503–510.

Tsukruk, V. V. & Bliznyuk, V. N. (1998). Adhesive and friction forces between chemically modified silicon and silicon nitride surfaces. *Langmuir*, *14*, 446–455.

Verdaguer, A., Santos, S., Sauthier, G., Segura, J. J., Chiesa, M., & Fraxedas, J. (2012). Water-mediated height artifacts in dynamic atomic force microscopy. *Physical Chemistry and Chemical Physics*, *14*, 16080–16087.

Vesenka, J., Manne, S., Giberson, R., Marsh, T., & Henderson, E. (1993). Colloidal gold particles as an incompressible atomic force microscope imaging standard for assessing the compressibility of biomolecules. *Biophysical Journal*, *65*, 992–997.

Wnęk, M., Górzny, M. Ł., Ward, M. B., Wälti, C., Davies, A. G., Brydson, R., Evans, S. D., & Stockley, P. G. (2013). Fabrication and characterization of gold nano-wires templated on virus-like arrays of tobacco mosaic virus coat proteins. *Nanotechnology*, *24*, 025605–025612.

Xu, X., Carrasco, C., De Pablo, P. J., Gomez-Herrero, J., & Raman, A. (2008). Unmasking imaging forces on soft biological samples in liquids when using atomic force microscopy: A case study on viral capsids. *Biophysical Journal*, *95*, 2520–2528.

Zahr, O. K. & Blum, A. S. (2012). Solution phase gold nanorings on a viral protein template. *Nano Letters*, *12*, 629–633.

Zaitlin, M. & Israel, H. 1975. Tobacco mosaic virus (type strain). In Commonw Mycol Inst/Assoc Appl Biol Kew, England. descriptions of plant viruses n° 151.

Zhao, Y., Ge, Z., & Fang, J. (2008). Elastic modulus of viral nanotubes. *Physical Review E*, *78*, 031914–031919.

SUPPORTING INFORMATION

Additional Supporting Information may be found in the online version of this article.